Non-invasive surface-stripping for epifluorescence small animal imaging

Sophie Piper,[1,*] Peyman Bahmani,[2] Jan Klohs,[2,5] Riad Bourayou,[6] Peter Brunecker,[3] Jochen Müller,[2] Denise Harhausen,[2] Ute Lindauer,[2,4] Ulrich Dirnagl,[2,3] Jens Steinbrink,[1,3,7] Andreas Wunder[2,3,7]

[1]*Berlin Neuroimaging Center, Charité University Medicine Berlin, Charitéplatz 1, 10117 Berlin, Germany*
[2]*Experimental Neurology, Charité University Medicine Berlin, Charitéplatz 1, 10117 Berlin, Germany*
[3]*Center for Stroke Research, Charité University Medicine Berlin, Charitéplatz 1, 10117 Berlin, Germany*
[4]*Currently with the Department of Neurosurgery, Klinikum rechts der Isar, Technical University Munich, Ismaninger Str. 22, 81675 Munich, Germany*
[5]*Currently with the Institute for Biomedical Engineering, University of Zurich and ETH, Wolfgang-Pauli-Str. 10, CH-8093 Zürich, Switzerland*
[6]*German Heart Institute, Augustenburgerplatz 1, 13353 Berlin, Germany*
[7]*These authors contributed euqually to this work.*
**sophie.piper@charite.de*

Abstract: Non-invasive near-infrared fluorescence (NIRF) imaging is a powerful tool to study pathophysiology in a wide variety of animal disease models including brain diseases. However, especially in NIRF imaging of the brain or other deeper laying target sites, background fluorescence emitted from the scalp or superficial blood vessels can impede the detection of fluorescence in deeper tissue. Here, we introduce an effective method to reduce the impact of fluorescence from superficial layers. The approach uses excitation light at two different wavelengths generating two images with different depth sensitivities followed by an adapted subtraction algorithm. This technique leads to significant enhancement of the contrast and the detectability of fluorochromes located in deep tissue layers in tissue simulating phantoms and murine models with stroke.

OCIS codes: (0100.2980) Image Enhancement; (0110.2960) Imaging analysis.

References and links

1. F. Leblond, S. C. Davis, P. A. Valdés, and B. W. Pogue, "Pre-clinical whole-body fluorescence imaging: Review of instruments, methods and applications," J. Photochem. Photobiol. B **98**(1), 77–94 (2010).
2. V. Ntziachristos, "Fluorescence molecular imaging," Annu. Rev. Biomed. Eng. **8**(1), 1–33 (2006).
3. M. C. Pierce, D. J. Javier, and R. Richards-Kortum, "Optical contrast agents and imaging systems for detection and diagnosis of cancer," Int. J. Cancer **123**(9), 1979–1990 (2008).
4. A. Wunder, and J. Klohs, "Optical imaging of vascular pathophysiology," Basic Res. Cardiol. **103**(2), 182–190 (2008).
5. A. Wunder, R. H. Straub, S. Gay, J. Funk, and U. Müller-Ladner, "Molecular imaging: novel tools in visualizing rheumatoid arthritis," Rheumatology (Oxford) **44**(11), 1341–1349 (2005).
6. A. R. Hsu, L. C. Hou, A. Veeravagu, J. M. Greve, H. Vogel, V. Tse, and X. Chen, "In vivo near-infrared fluorescence imaging of integrin alphavbeta3 in an orthotopic glioblastoma model," Mol. Imaging Biol. **8**(6), 315–323 (2006).
7. C. M. McCann, P. Waterman, J. L. Figueiredo, E. Aikawa, R. Weissleder, and J. W. Chen, "Combined magnetic resonance and fluorescence imaging of the living mouse brain reveals glioma response to chemotherapy," Neuroimage **45**(2), 360–369 (2009).
8. V. Ntziachristos, C. H. Tung, C. Bremer, and R. Weissleder, "Fluorescence molecular tomography resolves protease activity in vivo," Nat. Med. **8**(7), 757–761 (2002).
9. M. Hintersteiner, A. Enz, P. Frey, A. L. Jaton, W. Kinzy, R. Kneuer, U. Neumann, M. Rudin, M. Staufenbiel, M. Stoeckli, K. H. Wiederhold, and H. U. Gremlich, "In vivo detection of amyloid-beta deposits by near-infrared imaging using an oxazine-derivative probe," Nat. Biotechnol. **23**(5), 577–583 (2005).
10. D. Hyde, R. de Kleine, S. A. MacLaurin, E. Miller, D. H. Brooks, T. Krucker, and V. Ntziachristos, "Hybrid FMT-CT imaging of amyloid-beta plaques in a murine Alzheimer's disease model," Neuroimage **44**(4), 1304–1311 (2009).

#129204 - $15.00 USD Received 1 Jun 2010; revised 24 Jun 2010; accepted 2 Jul 2010; published 14 Jul 2010

11. J. Klohs, N. Baeva, J. Steinbrink, R. Bourayou, C. Boettcher, G. Royl, D. Megow, U. Dirnagl, J. Priller, and A. Wunder, "In vivo near-infrared fluorescence imaging of matrix metalloproteinase activity after cerebral ischemia," J. Cereb. Blood Flow Metab. **29**(7), 1284–1292 (2009).
12. J. Klohs, M. Gräfe, K. Graf, J. Steinbrink, T. Dietrich, D. Stibenz, P. Bahmani, G. Kronenberg, C. Harms, M. Endres, U. Lindauer, K. Greger, E. H. Stelzer, U. Dirnagl, and A. Wunder, "In vivo imaging of the inflammatory receptor CD40 after cerebral ischemia using a fluorescent antibody," Stroke **39**(10), 2845–2852 (2008).
13. J. Klohs, J. Steinbrink, R. Bourayou, S. Mueller, R. Cordell, K. Licha, M. Schirner, U. Dirnagl, U. Lindauer, and A. Wunder, "Near-infrared fluorescence imaging with fluorescently labeled albumin: a novel method for non-invasive optical imaging of blood-brain barrier impairment after focal cerebral ischemia in mice," J. Neurosci. Methods **180**(1), 126–132 (2009).
14. J. Klohs, J. Steinbrink, T. Nierhaus, R. Bourayou, U. Lindauer, P. Bahmani, U. Dirnagl, and A. Wunder, "Noninvasive near-infrared imaging of fluorochromes within the brain of live mice: an in vivo phantom study," Mol. Imaging **5**(3), 180–187 (2006).
15. J. Laufer, E. Zhang, G. Raivich, and P. Beard, "Three-dimensional noninvasive imaging of the vasculature in the mouse brain using a high resolution photoacoustic scanner," Appl. Opt. **48**(10), D299–D306 (2009).
16. E. M. Hillman, "Optical brain imaging in vivo: techniques and applications from animal to man," J. Biomed. Opt. **12**(5), 051402 (2007).
17. S. A. Prahl, (2001), *http://omlc.ogi.edu/spectra/hemoglobin/index.html*.
18. L. Wang, S. L. Jacques, and L. Zheng, "MCML--Monte Carlo modeling of light transport in multi-layered tissues," Comput. Methods Programs Biomed. **47**(2), 131–146 (1995).
19. L. Wang, S. L. Jacques, and L. Zheng, "CONV--convolution for responses to a finite diameter photon beam incident on multi-layered tissues," Comput. Methods Programs Biomed. **54**(3), 141–150 (1997).
20. F. Bevilacqua, D. Piguet, P. Marquet, J. D. Gross, B. J. Tromberg, and C. Depeursinge, "In vivo local determination of tissue optical properties: applications to human brain," Appl. Opt. **38**(22), 4939–4950 (1999).
21. C. Meisel, K. Prass, J. Braun, I. Victorov, T. Wolf, D. Megow, E. Halle, H. D. Volk, U. Dirnagl, and A. Meisel, "Preventive antibacterial treatment improves the general medical and neurological outcome in a mouse model of stroke," Stroke **35**(1), 2–6 (2003).
22. E. E. Graves, D. Yessayan, G. Turner, R. Weissleder, and V. Ntziachristos, "Validation of in vivo fluorochrome concentrations measured using fluorescence molecular tomography," J. Biomed. Opt. **10**(4), 044019 (2005).
23. R. Bourayou, H. Boeth, H. Benav, T. Betz, U. Lindauer, T. Nierhaus, J. Klohs, A. Wunder, U. Dirnagl, and J. Steinbrink, "Fluorescence tomography technique optimized for noninvasive imaging of the mouse brain," J. Biomed. Opt. **13**(4), 041311 (2008).
24. M. Gao, G. Lewis, G. M. Turner, A. Soubret, and V. Ntziachristos, "Effects of background fluorescence in fluorescence molecular tomography," Appl. Opt. **44**(26), 5468–5474 (2005).
25. A. J. Chaudhari, S. Ahn, R. Levenson, R. D. Badawi, S. R. Cherry, and R. M. Leahy, "Excitation spectroscopy in multispectral optical fluorescence tomography: methodology, feasibility and computer simulation studies," Phys. Med. Biol. **54**(15), 4687–4704 (2009).

Introduction

A growing number of animal experimental studies show that non-invasive near-infrared fluorescence (NIRF) imaging can be successfully used for specific visualization of biological processes in a wide variety of animal disease models [1,2] including models for cancer [3], vascular disease [4] or arthritis [5]. The technique has also been applied for studying brain pathologies such as brain tumors [6–8], neurodegenerative diseases [9,10], or cerebral ischemia [11–13]. Various methodological challenges have to be considered when applying non-invasive NIRF imaging to animal models of brain disease or other deeper laying targets in general. Due to extinction in tissues, the number of excitation photons reaching a deep-seated fluorescence site and the subsequent number of fluorescence photons reaching back the surface decreases nonlinearly with the depth of the fluorescent object of interest. NIRF epi-illumination imaging is inherently highly sensitive to fluorescent sources in superficial layers. Thus, the non-invasive visualization of compound binding or uptake within deeper tissue mingles with strong superficial background signals [13,14]. In the particular case of planar fluorescence imaging of the murine head, these signals originate from large vessels on the dorsal surface of the brain [15] and the highly vascularized scalp, skull bone, and dura mater.

Addressing this issue, we here describe and validate a technique to improve the contrast of non-invasive fluorescence images using the example of the murine brain by subtracting the contribution of unspecific fluorescence coming from superficial structures using two different excitation wavelengths, 670 nm and 633 nm. We have done Monte-Carlo simulations to mimic the depth-dependent sensitivity of different excitation wavelengths in an epi-illumination NIRF imaging system and tested this 'non-invasive surface-stripping' approach

#129204 - $15.00 USD Received 1 Jun 2010; revised 24 Jun 2010; accepted 2 Jul 2010; published 14 Jul 2010

in i) tissue simulating phantoms and in live mice with ii) an implanted fluorescent capsule or iii) with stroke.

Theory

In the wavelength range discussed here, blood is the most relevant absorber. At 633 nm the absorption coefficient of hemoglobin is a factor 2-5 higher than at 670 nm [16,17], thus the associated fluorescence image owns a stronger relative weight for the fluorescence from superficial layers than the fluorescence image obtained for an excitation at 670 nm. In a simplistic model, we can describe a deep laying fluorescing inclusion with a concentration c^{deep}, while fluorescent sources from superficial layers shall be represented by c^{surf}. At two different wavelengths the fluorescence detected in an epi-illumination fluorescence imaging system is

$$I_{633nm}^{fluo} = \alpha_1 \left(S_{633nm}^{surf} c^{surf} + S_{633nm}^{deep} c^{deep} \right)$$

$$I_{670nm}^{fluo} = \alpha_2 \left(S_{670nm}^{surf} c^{surf} + S_{670nm}^{deep} c^{deep} \right) \quad (1)$$

I_{λ}^{fluo} is the measured fluorescence intensity per image voxel in J/cm^{2}s, S_{λ}^{surf} and S_{λ}^{deep} are the sensitivities for wavelength λ_i in J•L/(cm^{2}s mol), α_1 and α_2 are coupling coefficients and c^{surf}, c^{deep} are the mean fluorophore concentrations in mol/L for the superficial layers and the inclusion depth, respectively. A difference image $\hat{I}$ of both fluorescence images [Eq. (1)] can be defined, potentially reducing the influence of the superficial layers

$$\hat{I} = I_{670nm}^{fluo} - \beta \cdot I_{633nm}^{fluo} \quad (2)$$

When β is chosen $\beta = (\alpha_2 S_{670nm}^{surf})/(\alpha_1 S_{633nm}^{surf})$, the difference image [Eq. (2)] will be

$$\hat{I} = c^{deep} \cdot \alpha_2 \left(S_{670nm}^{deep} - \frac{S_{670nm}^{surf}}{S_{633nm}^{surf}} S_{633nm}^{deep} \right). \quad (3)$$

In Eq. (3) the difference image $\hat{I}$ is no longer a function of c^{surf} but is now dependent only on the concentration of the inclusion c^{deep} and a proportionality constant α_2. The latter could be determined using a calibration phantom with a known fluorochrome concentration.

In practice, however, neither the sensitivities nor the coupling coefficients α_1 or α_2 are known, so a different way is needed to determine β. If prior knowledge of the fluorophore distribution is not available, β can be defined using histogram equalization (HE) of both fluorescence images. Here we assume the inclusion to be focal and the major part of both image intensities to be similarly distributed. HE transforms the signal intensity of the entire image acquired at 633 nm excitation wavelength to the same order of magnitude of signal level as the 670 nm image. Thus the difference between the two images after HE is mainly due to the focal inclusion of an unknown position in the brain. A histogram equalized subtraction thus allows the determination of $\hat{I}$, which is a brain weighted fluorescence image where signal intensities coming from superficial layers are highly reduced as they contribute to both fluorescence images excited at 670 nm and 633 nm, respectively.

Methods

Monte Carlo Simulation

To estimate the penetration depth at the two excitation wavelengths sensitivity factors were calculated with the help of a Monte Carlo simulation program developed by L.Wang and S.Jacques [18,19]. The simulation propagates photons in three dimensions and records photon deposition, A(x, y, z) in J/cm^3, due to absorption in each grid element of a spatial array. We calculated the responses to a finite 710 nm photon beam with a radius of 0.03 cm and two flat beam geometries at 633 nm and 670 nm, with a radius of 1.5 cm each, impinging on a slab, homogenous half space. Multiplying the latter two measures by the first mimics the spread

#129204 - $15.00 USD Received 1 Jun 2010; revised 24 Jun 2010; accepted 2 Jul 2010; published 14 Jul 2010

excitation of a light source in a fluorescence topography system and the detection of fluorescence light with a camera system. For every wavelength, we simulated 107 photons using a voxelsize of 0.006 cm^3, the anisotropy factor g was assumed to be 0.9 and the scattering coefficients μs_{633nm} = 0.22 /mm, μs_{670nm} = 0.20/mm and μs_{710nm} = 0.18/mm were taken from [20]. The used absorption properties of μa_{633nm} = 0.027/mm, μa_{670nm} = 0.014/mm and μa_{710nm} = 0.0095/mm correspond to a total cerebral hemoglobin concentration of 60µmol/L, with an oxygen saturation of 70%, dissolved in water based on the molar extinction coefficients published by Scott Prahl [17].

Fluorescence reflectance imaging

NIRF imaging was performed using a system developed by our group whereby fluorescence epi-illumination images can be taken at different excitation wavelengths without moving the animal [14]. Light from two TE-cooled laser diodes emitting 670 nm and 633 nm (Roithner Lasertechnik, Vienna, Austria) was coupled to an optical switch (LightTech Fiberoptics Inc, San Leandro, CA) and directed into a dark chamber, where it illuminated the object from above. A back-illuminated nitrogen-cooled CCD camera (Vers Array 512, 512 x 512 px, Roper Scientific Inc., Duluth, GA) with a focusing lens system (Nikkor macro lens, f = 50 mm, f/1.2, Nikon, Duesseldorf, Germany) and two 710-nm interference filters (FWHM 20 nm, Andover Corp., Salem, NH) detected the emitted fluorescence light.

Tissue phantom

The first column of Fig. 2 sketches the measurement set-up for the tissue phantom. We embedded a 2 mm long translucent polyethylene capsule (outer diameter of 0.61 mm, inner diameter of 0.26 mm, net volume 0.1 ml, SIMS Portex Ltd, Kent, UK) containing 10^{-12} mol of the fluorophore Cy5.5 (Cy5.5-dextran, Nanocs, New York, NY) beneath one or two layers of pork meat (4 mm each) with and without an additional top layer of fluorophore concentration (Cy5.5-dextran, Nanocs, New York, NY).

In-vivo model with implanted fluorescent capsule

In-vivo mouse model measurements were done with a mouse model described in detail in [14]. Translucent polyethylene tubes (outer diameter of 0.61 mm, inner diameter of 0.26 mm, SIMS Portex Ltd, Kent, UK) were filled with a Cy5.5-PEG solution (MW = 23 kDa, Nanocs, New York, NY). The tubes were cut into lengths of 2 mm and then thermally sealed containing a net volume of 0.1 ml and 10^{-12} mol Cy5.5.

An adult male C57Bl6 mouse weighing 25 g (Bundesinstitut fuer Risikoforschung, Berlin, Germany) was anaesthetized with a 5% solution of chloral hydrate (200 mg/kg) injected intraperitoneally. The hair was removed at the dorsal part of the head, the left temporalis muscle was detached, a hole was drilled into the skull and a capsule deposited at a depth of about 4 mm in the cortex of the left hemisphere approximately 2 mm caudal from bregma. The hole was closed using skin glue (Dermabond GmbH, Norderstedt, Germany) and muscle and skin were fixed into their original place. To simulate background fluorescence from fluorophores circulating in the vasculature, we injected 2 x 10^{-10} mol Cy5.5-PEG through the tail vein after the first set of NIRF measurements. After the bolus injection, the fluorophore concentration in the blood was approximately 0.1 µmol/L assuming a total blood volume of 2 mL in the mouse. The dye was allowed to equilibrate for 1 min before NIRF imaging [Fig. 3(a) and 3(b)].

In-vivo mouse model with stroke

The surface-stripping approach was also tested in-vivo with male C57Bl6/N mice that had undergone middle cerebral artery occlusion performed as previously published [12,21]. A monofilament was introduced into the common carotid artery under isoflurane anesthesia, advanced to the origin of the middle cerebral artery, and left there for 30 min, until reperfusion.

#129204 - $15.00 USD Received 1 Jun 2010; revised 24 Jun 2010; accepted 2 Jul 2010; published 14 Jul 2010

0.1 mg Cy5.5 labeled albumin (20µL of a 5% albumin solution with a Cy5.5 content of 387nm/mL, dissolved in 200µL NaCl, German Cancer Research Center Heidelberg) was injected intravenously 96 h after reperfusion. NIRF imaging was performed 2 h after injection of Cy5.5-albumin and the brain was then removed from the skull under deep anesthesia and used for ex vivo NIRF imaging [Fig. 4].

All procedures were in accordance with German animal welfare laws.

Data processing and image analysis

Data processing and analysis were performed using Matlab 6.5 software (The Mathworks, Inc., Natick, MA). An automatic baseline correction prior to analysis removed the read-out noise offset. All images were normalized to acquisition time and a top hat image (top hat filtering, structuring element circle with a diameter of 4 pixels) was subtracted from each image to correct for superficial fluorescence from dust. For illustration and comparison, all resulting fluorescence images were normalized to the maximum value of the fluorescence image, excited with 670 nm and smoothed by spatial filtering.

The surface-stripping algorithm

Before subtracting both fluorescence images excited with 633 nm and 670 nm, respectively, a histogram equalization (HE) was performed. The histogram of the fluorescence image I_{633nm} was stretched in steps to find the factor β_{HIS} that best minimizes the bounded area between the parametric representation of the histograms of I_{670nm} and $\beta_{HIS} \cdot I_{633nm}$. The difference ($I_{670nm} - \beta_{HIS} \cdot I_{633nm}$) was then calculated and negative pixel values of the adapted subtraction image were set at zero.

Results

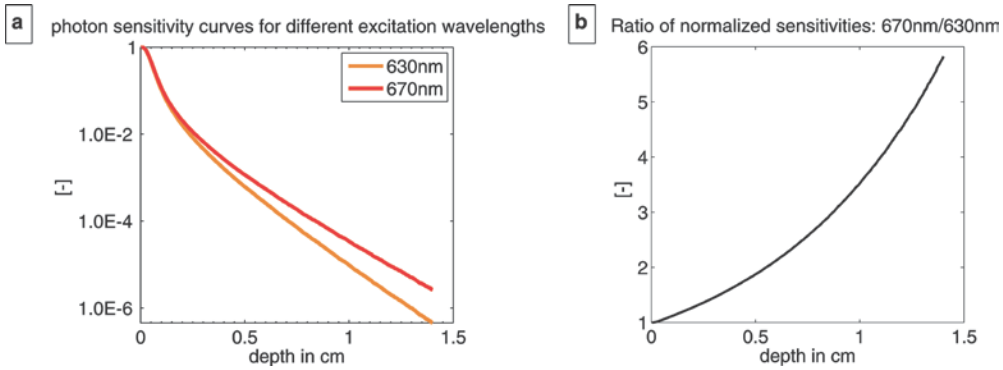

Fig. 1. Monte-Carlo results. (a) Normalized sensitivity in a logarithmic scale as a function of depth for a point inclusion fluorescing at 710 nm, spread excitation beams at 633 nm and 670 nm and a point-wise detection. This mimics the spread excitation of a fluorescent source in an epi-fluorescence imaging system and the detection with a camera system. (b) Quotient of the normalized sensitivities shown in (a).

The Monte Carlo results demonstrate the decrease in photon sensitivity with increasing depth for a point inclusion fluorescing at 710 nm and a point-wise detection when excited with spread excitation beams at 633 nm and 670 nm [Fig. 1(a)] and illustrate the very high sensitivity of epi-fluorescence images for dye concentrations in superficial layers. The ratio of these normalized sensitivities shows that the difference in inclusion signal intensity, between both excitation wavelengths grows exponentially with depth [Fig. 1(b)]. At an inclusion depth of 0.5 cm the fluorescence image excited with 670 nm is about a factor 2 more sensitive than the corresponding image excited with 633 nm, considering the same number of fluorescence photons being released by both excitation wavelengths.

#129204 - $15.00 USD Received 1 Jun 2010; revised 24 Jun 2010; accepted 2 Jul 2010; published 14 Jul 2010

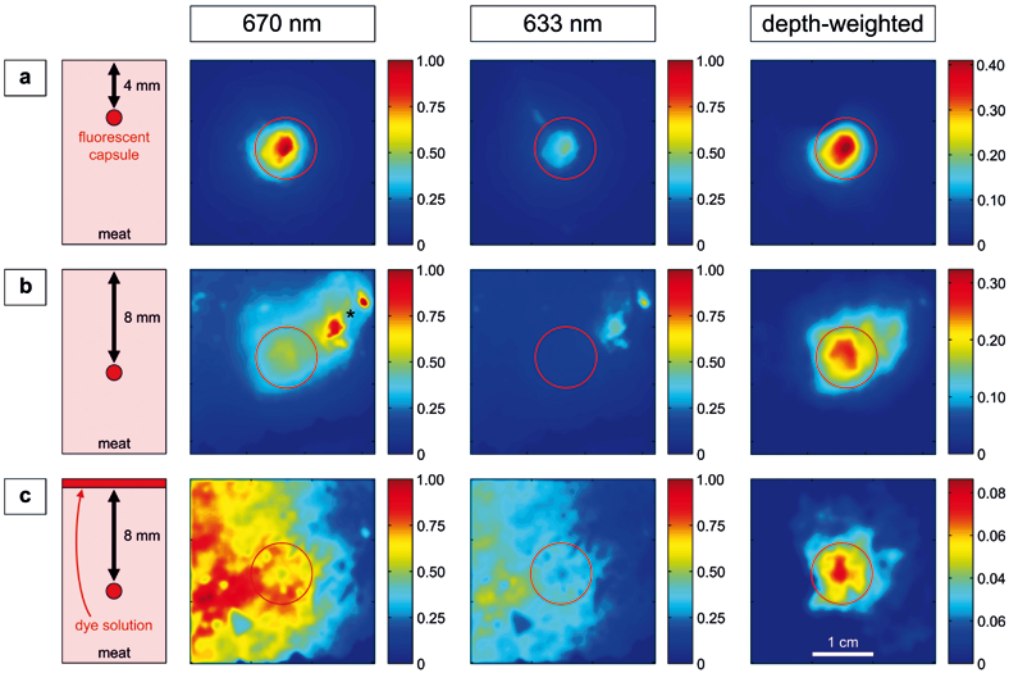

Fig. 2. Color-coded NIRF images of the tissue phantom study. Capsules containing NIRF dye Cy5.5 embedded in meat as sketched in a vertical view in the first column. Images with illumination at 670 (left) or 633 nm (middle), and the resulting depth-weighted images (right) are shown. The red circles indicate the position of the fluorescent target. (a) capsule located 4 mm below the surface. (b) capsule located 8 mm below the surface. The asterisk indicates an area of strong superficial tissue autofluorescence, which is strongly reduced in the depth-weighted image. (c) capsule located 8 mm below the surface and a dye solution is applied topically on the surface. The color bars represent relative fluorescence intensities (arbitrary units).

Figure 2 shows NIRF images of a capsule containing 10^{-12} mol of the NIR fluorochrome Cy5.5 in a tissue phantom. Three different experimental situations are sketched in the first column of the figure. In the first example [Fig. 2(a)], the capsule is covered by a 4 mm layer of pork meat. The capsule can be clearly seen in the raw fluorescence images excited with 670 nm and 633 nm, respectively, as well as in the histogram equalized subtraction image ('depth-weighted' image). In the second example [Fig. 2(b)], the inclusion is embedded in meat at a depth of 8 mm. Without prior knowledge, it cannot be univocally localized on either NIRF image. The detection of the fluorescent inclusion is further hampered by a superficial fluorescent signal in the upper right corner, as indicated by the asterisk. In the subtraction image, the unwanted superficial signals are strongly suppressed and the capsule can be clearly localized. When an NIRF dye solution is applied topically to increase the fluorescence at the very surface of the phantom [Fig. 2(c)], the 8 mm deep inclusion is only visible after the surface-stripping algorithm is applied. Notably, an improved contrast and a clear reduction of the effect of superficial layers can be observed in all cases.

#129204 - $15.00 USD Received 1 Jun 2010; revised 24 Jun 2010; accepted 2 Jul 2010; published 14 Jul 2010

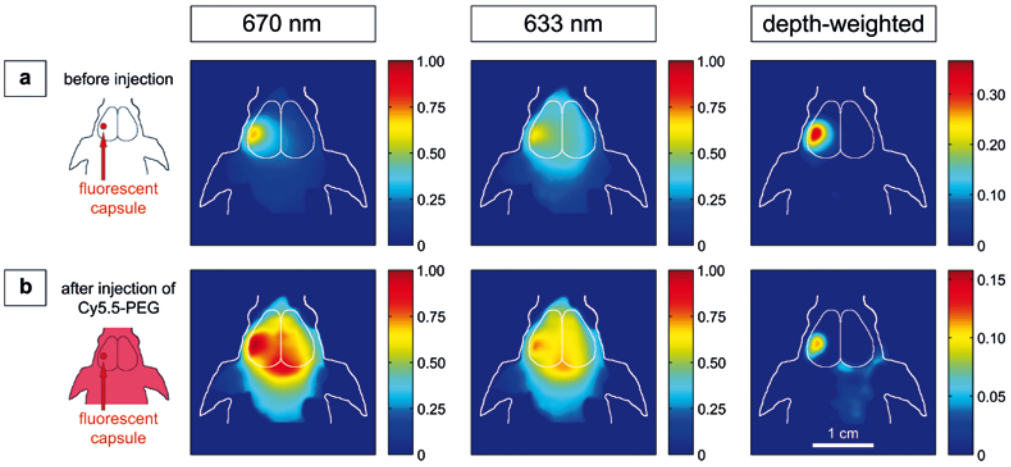

Fig. 3. Non-invasive NIRF images of a live mouse implanted with an intracranial capsule containing 10^{-12} mol Cy5.5-PEG. Images after illumination with light of 670 or 633 nm wavelengths, and the resulting depth-weighted images are depicted. (a) before and (b) after i.v.-injection of 2 x 10^{-10}mol Cy5.5-PEG.

Figure 3(a) and 3(b) show fluorescence images of a living mouse with a surgically implanted fluorescent capsule located about 4 mm deep into the left hemisphere of the brain. Before application of a long-circulating dye [Fig. 3(a)], the implanted capsule is visible after excitation at either wavelength. Ubiquitous background tissue fluorescence is further depleted after applying the subtraction scheme. After intravenous injection of 2 x 10^{-10} mol Cy5.5-PEG to increase background fluorescence [Fig. 3(b)], a mixed contribution from the capsule as well as from the confluens sinuum [confluence of superior sagittal and transverse venous sinuses] is observed. The latter cancels out almost completely after the 'non-invasive surface-stripping' algorithm: the rather diffuse fluorescence signal of the raw images is focused and localized to the area overlying the implanted capsule.

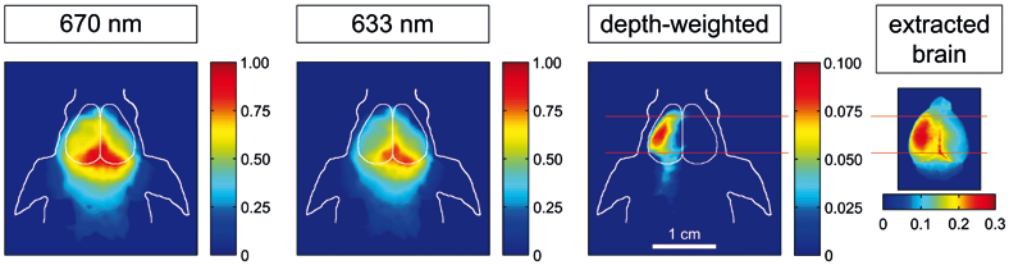

Fig. 4. Non-invasive NIRF images of a live mouse after experimentally induced cerebral ischemia in the left hemisphere 2 h after i.v.-injection of NIRF-labeled albumin.

Figure 4 demonstrates how the subtraction scheme facilitates the detection of a fluorescent compound accumulating in the diseased brain tissue in a mouse model of stroke. After experimentally inducing cerebral ischemia in a mouse, fluorescently labeled albumin, a marker for blood-brain barrier disruption, was injected intravenously. No detected fluorescence signal could be primarily attributed to the ischemic hemisphere at 670 or 633 nm excitation wavelengths, both images are dominated by the centered fluorescence signal from the confluens sinuum. After use of the technique presented in this paper, a focal NIRF signal emerged, which corresponds well with the location of the fluorescence over the ischemic area on the ex vivo image taken after removal of the skull.

#129204 - $15.00 USD Received 1 Jun 2010; revised 24 Jun 2010; accepted 2 Jul 2010; published 14 Jul 2010

Conclusion and discussion

Our new technique enables the visualization of fluorescent sources located deep in tissue layers where detection was previously hampered by strong fluorescence from superficial structures. In all experimental settings investigated, the application of this approach led to a significant increase of the contrast through subtraction of superficial signal components and therefore to an improved localization of the fluorescent source. This technique is simple to implement and highly relevant for studies using non-invasive NIRF imaging.

While we focused this article on showing the usefulness of the presented surface-stripping approach in the particular case of cerebral ischemia in the murine brain, the results of the phantom study [Fig. 2] indicate that this technique is not restricted to cerebral target sites. The demonstrated subtraction algorithm could also be helpful when applied in other experimental settings, where the signal of interest clearly lies in deeper tissues, e.g. the kidney.

The advantage of using a histogram equalization to determine β is that it is independent of modulations in the set-up such as changes of the excitation light intensity. However, future studies might show that the β value is stable for a certain set-up and a certain type of object.

A major limitation is that the presented subtraction algorithm reduces not only the interfering fluorescence signals from superficial structures, but inevitably also the target signal. A fluorescent source of interest in a superficial layer like e.g. in a tumor model, where tumor cells may grow from the brain into the scalp, would be removed or at least strongly attenuated by the 'surface-stripping' approach. However, in future a wavelength shorter than 633 nm could be applied and might allow taking advantage of a lower penetration of the excitation photons and hence confining excitation of fluorochromes to superficial layers.

In an in vivo animal model, fluorescence can originate also from structures not of interest. This can be caused by portions of the fluorochrome circulating in the vasculature. For example the residual fluorescence signal from the sinus junction in the depth-weighted image [Fig. 3(b)] likely stems from a deep lying vessel and is thus a source of background fluorescence from deeper layers.

Here, we used an epi-illumination imaging system and this geometry does not allow for quantification of fluorophore concentration in thick diffuse media. Even when using the 'surface-stripping' technique proposed in this article, only relative changes in fluorescence can be obtained. Therefore, we cannot quantify how deep 'superficial' really is and to which extent the subtraction method cuts off also the signal of interest. Modeling tissue optics would help evaluating the usefulness and limitations of the presented subtraction algorithm. Nevertheless, the method could be possibly applied to tomographic approaches, using only the subtraction images for 3D image reconstruction. Other investigators dealing with fluorescence background signals in the blood system of mice have improved accuracy of quantitation by subtracting a constant [22,23] or a distance-dependent average [24] background fluorescence signal from the data before tomographic reconstruction. In contrast, our adaptive subtraction algorithm reduces especially superficial fluorescent background sources, depending on their anatomical position. This might further improve image quality and quantification accuracy when applied to optical tomography. Regarding the use of more than one wavelength in optical tomography, promising results have been presented recently by applying multi-spectral excitation and detection [25].

In conclusion, our data demonstrate that using the 'non-invasive surface-stripping' algorithm improves the visualization of fluorescent sources in deep tissue layers despite high background signals from superficial sources. Notably, the technique can reveal fluorescent sources which would have escaped conventional NIRF imaging.

Acknowledgements

Supported by the European Union's Seventh Framework Programme (FP7/2008-2013) under grant agreements n° 201024 and n° 202213 (European Stroke Network), and the German Ministry for Health and Education, the Zukunftsfonds Berlin and the European Regional Development Fund (ERDF) of the EU. Furthermore we would like to thank Hans-Hermann

Schrenk and Eva Frei (German Cancer Research Center Heidelberg, Germany) for providing us with Cy5.5-HSA.

#129204 - $15.00 USD Received 1 Jun 2010; revised 24 Jun 2010; accepted 2 Jul 2010; published 14 Jul 2010